Chemistry Europe
European Chemical Societies Publishing

WILEY VCH

# Excellence in Chemistry Research


## Announcing our new flagship journal

- Gold Open Access
- Publishing charges waived
- Preprints welcome
- Edited by active scientists

## Meet the Editors of *ChemistryEurope*

**Luisa De Cola**
Università degli Studi di Milano Statale, Italy

**Ive Hermans**
University of Wisconsin-Madison, USA

**Ken Tanaka**
Tokyo Institute of Technology, Japan

Analytical Chemistry

# UiO-66/GO Composites with Improved Electrochemical Properties for Effective Detection of Phosphite(P(III)) in Phosphate(P(V)) Buffer Solutions

Ying Yang[+],[a] Wangui Wu[+],[a] Ziyan Wang,[a] Limei Huang,[a] Xiuling Ma,*[a] Zhangjing Zhang,[a, b] and Shengchang Xiang*[a, b]

Measurement of phosphorus is of great significance because it is a key element responsible for eutrophication in water environment. More efforts have been devoted to sensor-based detection of phosphate (P(V)), while few reports on that of phosphite (P(III)) are available due to the interferences from phosphate and/or other species. Here we synthesized UiO-66/graphene oxide (GO) composites and first observed that the cooperative utilization of UiO-66 and GO may provide a promising strategy to improve the electrochemical performances of MOF hybrid materials for effective detection of phosphite (P(III)) in phosphate (P(V)) buffer solutions (PBS). The current value of the oxidation peak is proportional to the phosphite concentration over the range of 10 μmol $L^{-1}$ - 500 μmol $L^{-1}$, and the limit of detection is 0.33 μmol $L^{-1}$ (S/N = 3) with the lowest value among the reported works.

## 1. Introduction

Phosphorus (P) is a key factor limiting nutrient for eutrophication which is of great environmental and scientific concern.[1] Therein, phosphate P(V) is considered as the main carrier of phosphorus, and phosphite P(III) can be converted into phosphate through biological and abiotic pathways.[2] Therefore, phosphite is also an important nutrient carrier to support the growth of algae,[3] and it has been found in drinking water, lakes, and industrial waste-water.[4] At present, traditional analytical techniques such as spectrophotometry,[5] as well as chromatography including ion chromatography,[6] and high-performance liquid chromatography,[7] are mainly used for the determination of phosphite. These methods exhibit their excellent performance except for cost and time for pretreatment of samples. Currently, sensors have drawn people's attention due to simple operation, low cost, high sensitivity, and environmental friendliness.[8] More efforts have been devoted to sensor-based detection of phosphate (P(V)), while few reports on phosphite (P(III)) are available because of the interferences from phosphate and/or other species, which is difficult to overcome.[9] Although the electrochemical detection methods of P(III) has been developed,[10] it is still lack of relevant research on the determination of (P(III)) in the presence of P species. Therefore, it is crucial to develop an alternative P(III) electrochemical sensor which could effectively confront the unavoidable interferences from phosphate and/or other species.

As a member of crystalline porous materials, metal-organic frameworks (MOFs) that can be assembled through metal ions or clusters and organic linkers, have attracted extensive attention.[11] Recently, important progress has been made in the application of electrochemical sensors owing to the development of nanostructure MOFs.[12] As a typical MOFs material, UiO-66 ($Zr_6O_4(OH)_4(BDC)_{12}$) with a crystalline structure constituted by hexametric $Zr_6O_{32}$ units was demonstrated to have high chemical and thermal stability, as well as excellent absorbability.[13] Therefore, more applications of UiO-66 and its derivatives or composites have been developed, such as adsorption and separation,[13a] photocatalysis,[13b] proton conductivity,[14] and electrochemical sensor.[15] In especial, the reported UiO-66/modified straw nanocomposites show excellent adsorption and removal of phosphate in water,[16] which means that it is potential for UiO-66 to construct electrochemical sensors for detecting P in environmental waters. However, UiO-66 with spherical structure is easy to be agglomerated as electrode materials. It is essential to select a special material complex with UiO-66 to overcome the poor dispersion and improve the P electrochemical sensing performance.

The designing of new electrochemical sensors with desirable analytical and electrochemical features can be obtained to exploit for ordinary environmental sensing systems by modifying the electrode surface with various hybrid materials.[17] Based on graphene oxide (GO) possessing large surface area, high electronic conductivity and ion absorption,

[a] Y. Yang,[+] W. Wu,[+] Z. Wang, Dr. L. Huang, Dr. X. Ma, Prof. Z. Zhang, Prof. S. Xiang
Fujian Provincial Key Laboratory of Polymer Materials, College of Chemistry and Materials Science, Fujian Normal University, 32 Shangshan Road, Fuzhou 350007, PR China
E-mail: xlma@fjnu.edu.cn
scxiang@fjnu.edu.cn
[b] Prof. Z. Zhang, Prof. S. Xiang
State Key Laboratory of Structural Chemistry, Fujian Institute of Research on the Structure of Matter, Chinese Academy of Sciences, Fuzhou, Fujian 350002, PR China
[+] These authors contributed equally to this work.

Supporting information for this article is available on the WWW under https://doi.org/10.1002/slct.202002594

and good catalytic performance, the introduction of GO to UiO-66 was performed to fulfill our expectation in this work. According to the reported works, diverse GO composites were explored and used in drug delivery,[18] sewage treatment,[19] solar cell,[20] electrochemical sensor[21] and so on. Also, GO composites based on MOFs were developed and applied in various fields, such as biogas decarburization,[22] proton exchange membranes[23] and electrochemical sensor.[24] The MOFs/GO composites are highly dispersible and stable for an electrochemical sensing application, and the modified electrode has higher sensitivity and stronger anti-interference capability compared with the GO modified electrode alone.[24] Therefore, the composites show great attraction to electrochemistry and could be developed as potential electrode materials for sensing inorganic acid ion, although their application to inorganic ion has not been reported.

Given that the excellent absorbability of UiO-66, the high conductivity of GO, and the good dispersion and stability of MOFs/GO composites, UiO-66/GO composites prepared by simple blending technology were used as electrode material to realize the desired purpose of electrochemical sensing P(III) in the presence of P(V) in this work. As expected, the signal-strength effect of UiO-66/GO/GCE was more remarkable than that of UiO-66/GCE or GO/GCE (shown in Figure 1). The linear range of P(III) on UiO-66/GO/GCE is 10–500 $\mu mol\,L^{-1}$ with the limit of detection (LOD) of 0.33 $\mu mol\,L^{-1}$ in 0.1 $mol\,L^{-1}$ phosphate buffer solutions (PBS) at pH values of 7. In terms of the LOD, the proposed sensor outperforms the reported electrochemical sensors constructed by palladium film with the LOD of 3.67 $\mu mol\,L^{-1}$[8c] and by hydroxyapatite with the LOD of 5.5 $\mu mol\,L^{-1}$.[8b] Our work developed a electrochemical sensor for the determination of P(III) in the presence of unavoidable interference P(V).

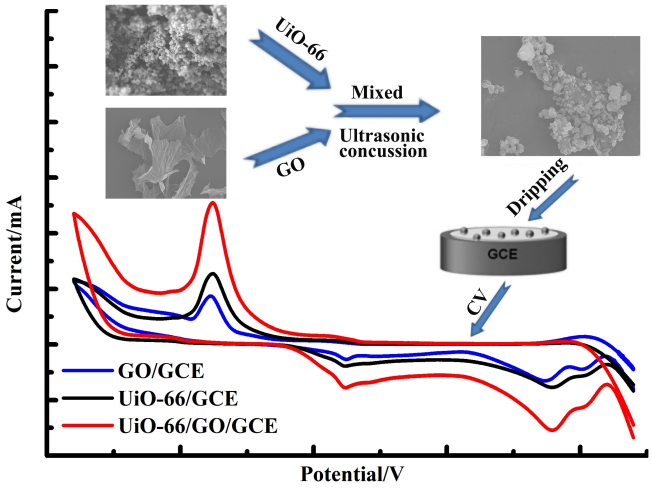


**Figure 1.** The construction process of UiO-66/GO/GCE and its performance to improve the electrochemical signals of phosphite.

## 2. Results and discussion

### 2.1. Characterization of the prepared materials

The prepared materials were characterized by the following means. By XRD measurements (shown in Figure 2a), the 2θ diffraction peaks of the prepared UiO-66 in accord with that of the simulated one at 7.397°, 8.534°, 12.062°, 17.076°, 22.230°, 25.747° correspond to the (111), (002), (022), (004), (115), (006) crystal planes of UiO-66 respectively,[25] indicating that UiO-66 was successfully prepared. Similarly, the peak of the synthesized GO at 11.2° is identical to that of the simulated characteristic diffraction peaks of GO. Moreover, it can be seen that the UiO-66/GO composites are contained characteristic diffraction peaks of UiO-66 and GO, and there was no shift in the diffraction peaks of UiO-66/GO compared with UiO-66, which shows that UiO-66 in the composites still maintains the high degree of crystallinity. TGA was used to investigate the thermal behavior of UiO-66, GO and UiO-66/GO in a nitrogen atmosphere. As shown in Figure 2b, to the UiO-66, the weight loss between 50 and 150 °C is mainly assigned to the release of the adsorbed water, while the weight loss between 200 and 300 °C is ascribed to the decomposition of DMF. Then, the mass loss between 480 and 600 °C is observed due to the collapse of the structure. It shows that UiO-66 has excellent thermal stability. From the curve of GO, the slight mass loss that occurred before 100 °C is related to the evaporation of water in GO interlayer. In agreement with Ref. [22], GO is thermally unstable and undergoes a rapid mass drop on heating to about 200 °C because of the loss of oxygen-containing groups. Compared with UiO-66 and GO, the mass loss of UiO-66/GO from 200 to 250 °C is more than that of UiO-66 and less than that of GO, which may be caused by the separation of oxygen-containing functional groups in the GO layer and the decomposition of DMF in the UiO-66 layer. Additionally, the composites have higher decomposition and collapse temperatures (up to 520 °C) than their parent materials. UiO-66/GO composites are the few reported examples with enhanced thermal stability using the GO hybrid approach, which is for the reason that the strong interactions between GO and UiO-66 reinforce the stability of the composite.[22]

Figure 2c shows the FT-IR spectra of GO, UiO-66, and UiO-66/GO, respectively. For UiO-66, the two sharp peaks at 1586 and 1401 $cm^{-1}$ can be attributed to the asymmetrical and symmetric stretching vibration of the carboxyl, respectively. The peaks at 746 and 665 $cm^{-1}$ correspond to the bending vibration modes of C–H. The FT-IR spectrum of GO exhibits the typical absorption peaks of its functional groups at 1045, 1225, 1400, 1623, and 1720 $cm^{-1}$, corresponding to C–O–C stretching, phenolic C-OH stretching, carboxylic C-OH stretching, C=C stretching and C=O stretching vibrations of carboxyl, respectively.[23] The functional peaks of UiO-66 or GO almost exist in UiO-66@GO composites, while the characteristic adsorption peaks intensity of partial oxygen-containing functional groups decrease or even disappear in the spectrum of composites, owing to the coordination between the carboxyl groups of GO and $Zr^{4+}$. In order to further demonstrate the successful blending of UiO-66 and GO, the element analysis

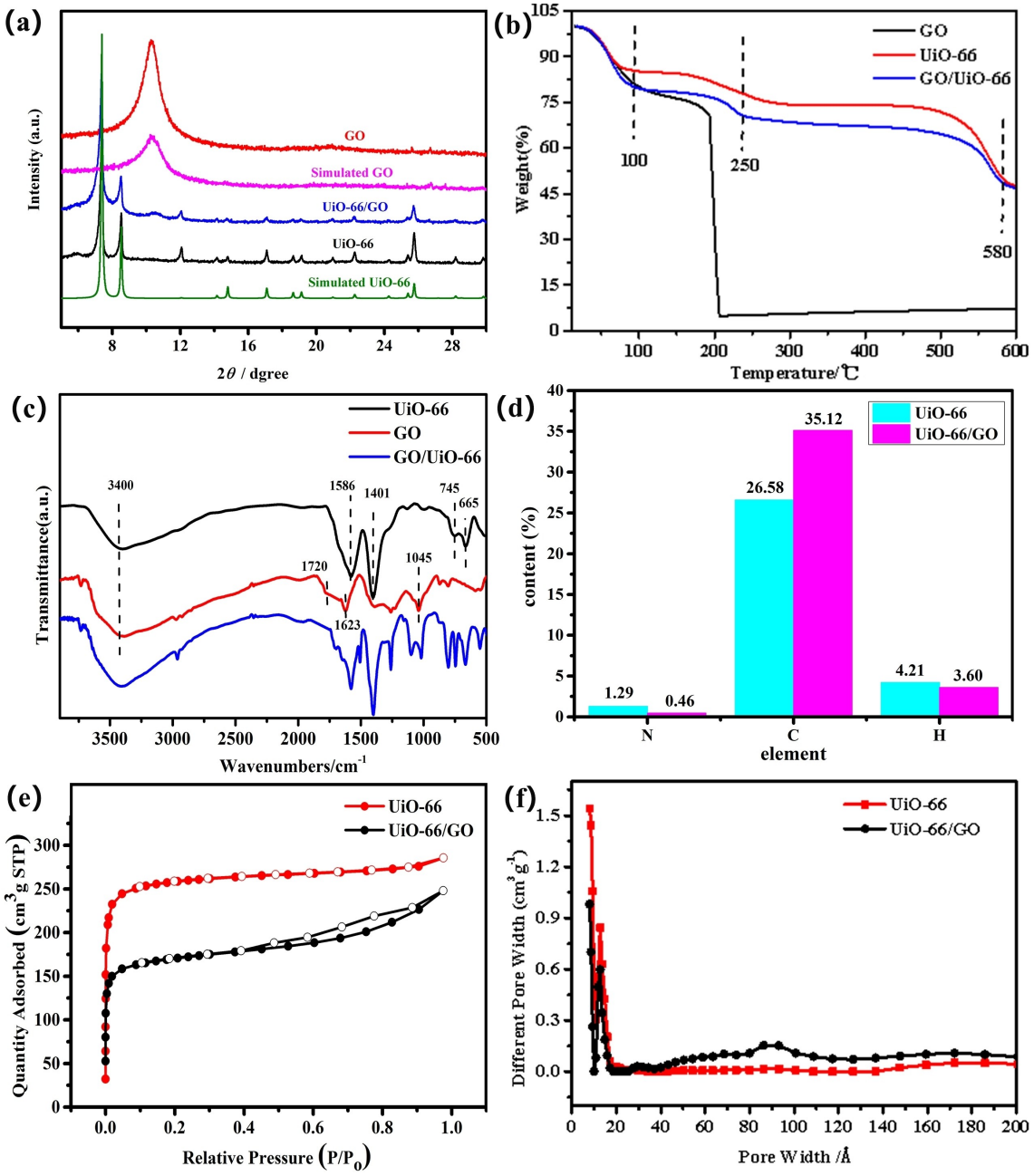


**Figure 2.** XRD patterns (a), TGA curves (b) and FT-IR curves (c) of UiO-66, GO and UiO-66/GO. Elemental contents (d), 77 K $N_2$ sorption isotherms (e) and pore-size distribution (f) of UiO-66 and UiO-66/GO.

were shown in Figure 2d. It can be seen that the C content of UiO-66 /GO composites is obviously higher than that of UiO-66 owing to the successful blending.

To evaluate the effect of doping GO on the pore properties of UiO-66, nitrogen adsorption-desorption isotherms and the corresponding pore size distributions of UiO-66 and UiO-66/GO were analyzed in Figure 2e and 2f. The isotherms of UiO-66 can be classified as the type I isotherm curve, which confirm that UiO-66 is a kind of microporous materials. The isotherms of UiO-66/GO are a type IV curve with an hysteresis loop (Figure 2e), indicating that it has mesoporous structures. Brunauer- Emmett-Teller (BET) surface areas of UiO-66 and UiO-66/GO are 866.4 and 557.7 $m^2/g$, respectively. Non-local-density functional theory (NLDFT) analysis was used to determine the pore size distributions of UiO-66 and UiO-66/GO (Figure 2f). The pore sizes of UiO-66 are below 2 nm assigned to the microporous material category. However, some pore sizes of UiO-66/GO are centered around 9 nm, and some below 2 nm, suggesting that UiO-66/GO belongs to the mesoporous material category as well as partially to the micropore category.

SEM was used to investigate the morphologies of UiO-66, GO and UiO-66/GO composites, as shown in Figure 3. It could

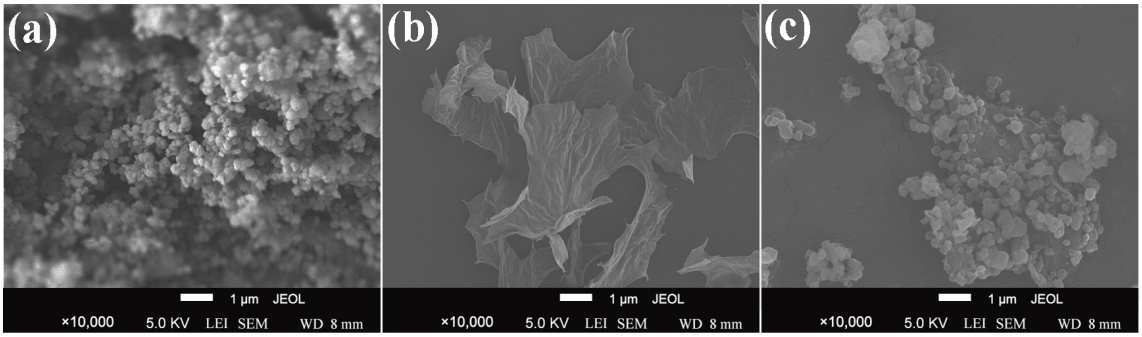


**Figure 3.** SEM images of UiO-66 (a), GO (b) and UiO-66/GO (c).

be seen that the appearance of UiO-66 is spherical (Figure 3a), and GO (b) shows irregular lamellar patterns (Figure 3b). With regard to UiO-66/GO composites, apparently, UiO-66 is effectively attached to the GO surface (Figure 3c).

### 2.2. Electrochemical characteristics of the modified electrodes

To assess the performance of the electrode modified by different materials, CV was used to study the electrochemical behavior of 10 μmol $L^{-1}$ phosphite at the electrodes in 0.1 mol $L^{-1}$ PBS (pH = 7.0). The obtained results are shown in Figure 4a. No matter which electrode was used, a significant oxidation peak at −0.8 V is observed, which is due to the oxidation of phosphite to phosphate, and phosphate shows weak-reduction to phosphite at 0.2 V. These results are consistent with Ref. [26]. Compared with GO/GCE and UiO-66/GCE, obviously, the oxidation peak current value of phosphite at UiO-66/GO/GCE is significantly higher than that at GO/GCE or UiO-66/GCE. That is, the electrochemical performance of the UiO-66/GO is obviously superior to UiO-66 and GO. The above results suggest that the UiO-66/GO has more excellent electrochemical activity for phosphite and it could be applied to selective determination of phosphite in the presence of P(V). According to the reported Ref. [16], UiO-66-based nanocomposites show excellent adsorption of P in water via forming Zr-O–P coordination bonds. What's more, the selected GO with large surface area, high electronic conductivity and ion absorption, and good catalytic performance might be favorable to overcome the poor dispersion of UiO-66 and improve the P electrochemical sensing performance. Therefore, the prominent electroactivity of UiO-66/GO may be attributed to the synergism the high electron migration rate of GO[27] and the excellent absorption ability of UiO-66.[28] Additionally, the UiO-66/GO composites with the micro/mesoporous properties are beneficial to the dispersion of other components and thereby help to improve the activity of catalyst. Then UiO-66/GO was selected as the material to construct an electrochemical sensor of phosphite, and its electrochemical properties were further investigated in the following section.

To further characterize the interface properties of UiO-66/GO/GCE, EIS was conducted in a 5 mmol $L^{-1}$ $[Fe(CN)_6]^{3-/4-}$ solution containing 0.1 mmol $L^{-1}$ KCl. As shown in Figure 4b, the arc sizes for UiO-66/GO and the bare electrode decrease in turn at high frequency, indicating that the UiO-66/GO material could effectively improve the electron transmission rate on the electrode surface, which is also beneficial to the electrochemical determination of phosphate.

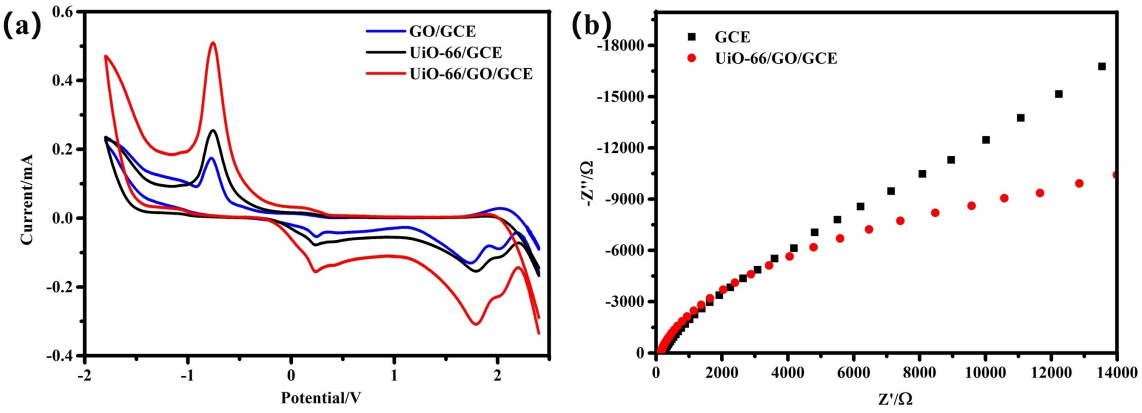


**Figure 4.** CV curves of 10 μmol $L^{-1}$ phosphite at the GO/GCE, UiO-66/GCE and UiO-66/GO/GCE in 0.1 mol $L^{-1}$ PBS (pH = 7.0) (a). EIS spectra of bare GCE and UiO-66/GO/GCE (b).

### 2.3. Effects of the dosage of GO, pH values, and scan rate

In this study, CV was conducted to investigate the influence of different conditions on the performance of UiO-66/GO/GCE.

The influence of GO doping amount on current response value of phosphite in PBS (pH = 7.0) with 10 μmol $L^{-1}$ phosphite was performed at different doses of GO (1, 2, 3, 4, 5 mg) on UiO-66/GO/GCE. As shown in Figure 5a, the current value of the oxidation peak increases first and then decreases with the increase of the doping amount. Among them, the oxidation peak current value reaches the maximum at the dosage of 2 mg. This may be because more electronic transmission happen and more catalytic active sites on the electron surface are generated with the dosage of GO increasing from 1 to 2 mg. However, the rise of the GO doping amount to 3 mg would hinder the mass transfer of phosphite because of the excessive thickness of the electrode surface film. Therefore, the GO doping amount of 2 mg was selected as the optimal doping amount.

Due to the proton-based participation in the electrochemical reactions of phosphite,[8c] it is necessary to further explore the effect of the electrolyte acidity on the electrochemical oxidation behavior of phosphite at UiO-66 /GO/GCE. As shown in Figure 5b, the oxidation peak current value of phosphite increases in the pH range of 4.5-7.0, reaching a maximum value at pH 7.0. Then, the current value of phosphite decreases with the increase in pH value d from 7.0 to 8.0. According to the reported work,[29] the stability of Zr-base MOFs fared poorly in alkaline solution, which is the reason that the NBO charge of oxygen atom in the hydroxyl ion group is more larger than that in carboxylate group, it means the stronger bond is formed between $OH^-$ and Zr (IV) than carboxylate and Zr (IV), and leading to the composition of Zr-base MOF under alkalinity condition. In addition, it is known that phosphite is a poly acid with pKa values of 1.3 and 6.6, and phosphite ions are deprotonated and more negative charges with the increase of pH value, which is not conducive to be adsorbed on UiO-66 through coulomb interaction. Moreover, the excessive $OH^-$ will compete with phosphite for the active sites under alkaline conditions, resulting in the reduction of the adsorption of phosphite.[30] Consequently, the adsorption effect is best and the oxidation peak current obtained is also strongest at the pH value of 7.0.

The effect of scan rate on UiO-66/GO/GCE in 0.1 mol $L^{-1}$ PBS (pH = 7.0) with 10 μmol $L^{-1}$ phosphite was performed. As shown in Figure 5c, the peak current values for phosphite at the potential range of −1–0.8 V increases with an increase of the scan rate from 10 to 100 mV $s^{-1}$. A good linear relationship between the oxidation peak current and scan rates was obtained, as shown in Figure 5d. The linear equation is $I_{pa}$ =

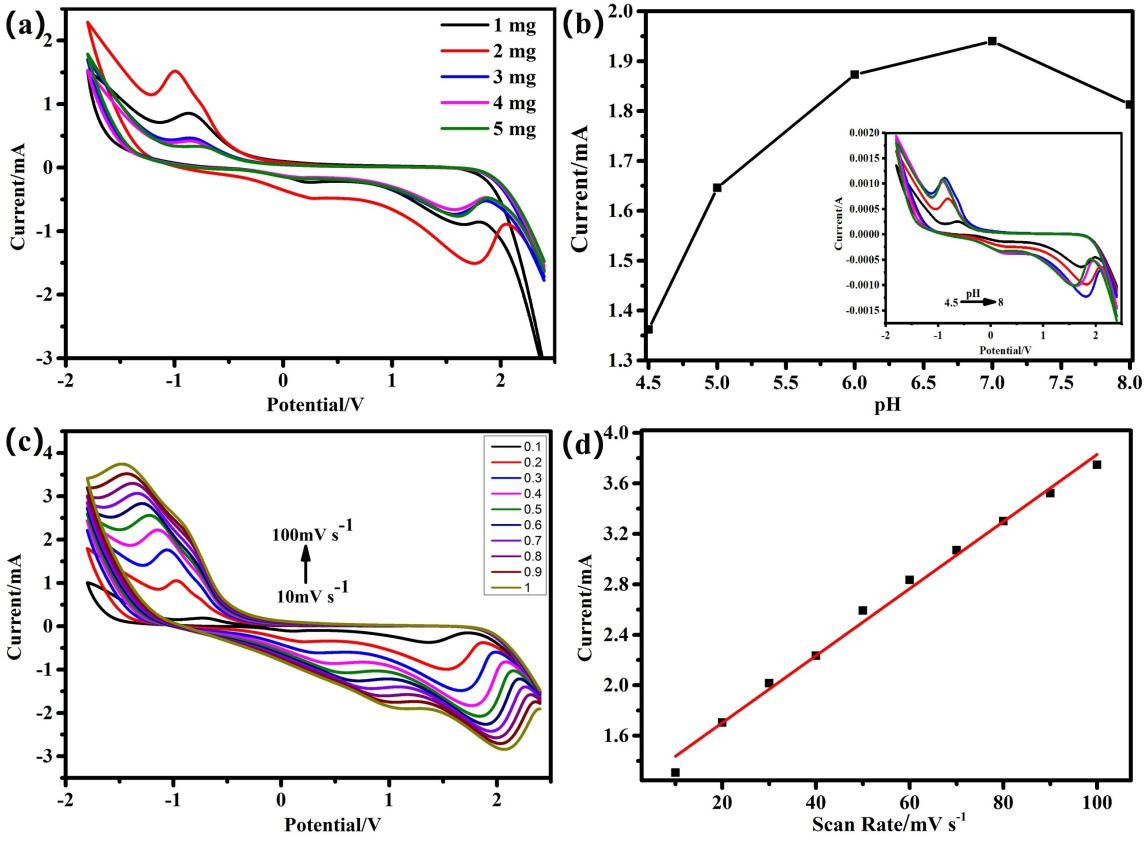


**Figure 5.** CV curves of different doping amounts at UiO-66/GO/GCE (a). The effect of pH on the oxidation peak current of phosphite (Insert is CV curves in PBS with different pH value) (b). CV curves of 10 μmol $L^{-1}$ phosphite at UiO-66/GO/GCE in 0.1 mol $L^{-1}$ PBS solution (pH = 7.0) with scan rates from 10 to 100 mV $s^{-1}$ (c). The linear relationship between oxidation peak current and scan rates (d).

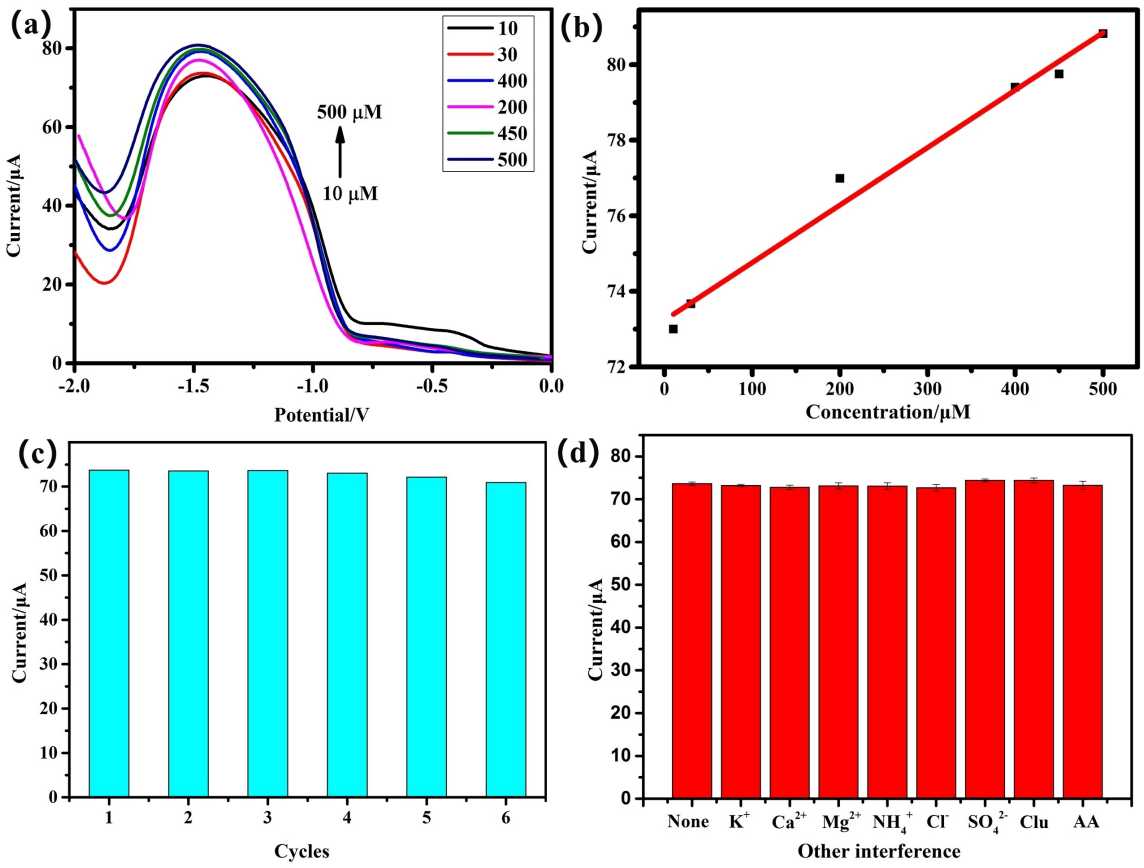


**Figure 6.** The DPV curves of UiO-66/GO/GCE in 0.1 mol $L^{-1}$ PBS (pH = 7.0) with different phosphite concentrations (a). Fitting curve of the peak current and target concentration (b). The regeneration (c) and the anti-interference (d) of UiO-66/GO/GCE in 0.1 mol $L^{-1}$ PBS (pH = 7.0) with 10 μmol $L^{-1}$ phosphite solutions.

$1.2 + 2.7 \times 10^{-2}$ $\nu$ with $R^2 = 0.993$. The results indicate that the electrode process of the oxidation reactions of phosphite at the UiO-66/GO/GCE is mainly controlled by adsorption. The reason may be that phosphite is oxidized to phosphate, and the complex reactions between phosphate ions and the hydroxyl group on the surface of UiO-66 easily take place, which could make phosphate being effectively trapped by UiO-66.

### 2.4. The performances of the UiO-66/GO /GCE

The linear ranges and LOD for phosphite on the UiO-66/GO/GCE were determined by DPV under the optimal experimental conditions. As shown in Figure 6a and b, the peak current of phosphite gradually increase with the increase of phosphite concentration from 10 μmol $L^{-1}$ to 500 μmol $L^{-1}$. The linear equation of the oxidation peak current value of phosphite is $I_{Pa}$ (μA) = $2.0 \times 10^{-2}$ $c$ (μmol $L^{-1}$) + 70 ($R^2 = 0.985$), and the LOD for phosphite is 0.33 μmol $L^{-1}$ (S/N = 3). As far as the LOD are concerned, except for ion chromatography, the method in this work outperforms the reported methods, including the electrochemical sensors constructed by palladium film with the LOD of 3.67 μmol $L^{-1}$ in 1.0 mol $L^{-1}$ sulfuric acid aqueous medium[8c] and by hydroxyapatite with the LOD of 5.5 μmol $L^{-1}$ in acetic acid/sodium acetate buffer solution.[8b] The comparisons of the reported literatures are shown in Table 1.

To evaluate the reproducibility of the constructed sensor, five parallel UiO-66/GO/GCE were prepared under the same conditions, and the current values of 10 μmol $L^{-1}$ phosphite at these parallel electrodes were determined by DPV in 0.1 mol $L^{-1}$

**Table 1.** Comparison for the determination phosphite by different methods.

| Determination methods | Linear range (μmol $L^{-1}$) | LOD (μmol $L^{-1}$) | Reference |
|---|---|---|---|
| Spectrophotometry | $4 \times 10^3$–$3.2 \times 10^4$ | 72 | [5] |
| High-performance liquid chromatography | $4 \times 10^4$–$1.44 \times 10^5$ | 6.08 | [7b] |
| Ion chromatography | 0.01–0.17 | 0.002 | [6a] |
| Fluorescent sensor (nickel oxide nanozyme) | 2–1000 | 1.46 | [8a] |
| Electrochemical senso (palladium film electrode) | 5–500 | 3.67 | [8c] |
| Electrochemical sensor (hydroxyapatite-based electrode) | $10$–$10^8$ | 5.5 | [8b] |
| Electrochemical sensor (UiO-66/GO/GCE) | 10–500 | 0.33 | This work |

PBS (pH = 7.0). The experimental results show the relative standard deviation (RSD) of 3.41%, which reveals an excellent reproducibility of the sensor. Regeneration is also one of the most important properties for the application of the sensor. Therefore, the sensor was immersed in water by shaking for 5 minutes, and back to the initial state. DPV was applied in the solutions containing 10 μmol $L^{-1}$ phosphite and 0.1 mol $L^{-1}$ PBS. The cycle was repeated using the above description. As shown in Figure 6c, the current values show minor change after six cycles, which indicate good durable performance. In addition, the stability of the UiO-66/GO/GCE was examined by storing at 4 °C refrigerator for one week. The results show that the peak current maintains 95.5% of the initial current before storage, indicating that the constructed sensor has a good stability.

Anti-interference studies were carried out in 0.1 mol $L^{-1}$ PBS containing 10 μmol $L^{-1}$ phosphite solutions by DPV (Figure 6d). There is almost no effect on the detection of phosphite in the presence of the P(V) and 100-fold concentration of $K^+$, $Ca^{2+}$, $Mg^{2+}$, $NH_4^+$, $Cl^-$, or $SO_4^{2-}$, or 50-fold concentration of glucose or ascorbic acid (AA). It illustrates that the developed sensor has a good anti-interference ability in the detection of phosphite.

The developed sensor was applied to the determination of phosphite in actual water samples collected from Minjiang River by DPV to assess the reliability of UiO-66/GO/GCE. The recovery test was carried out as Ref. [31]. As shown in Table 2, the recovery rates of phosphite are in the range of 97.9-99.3%. The results implied that UiO-66/GO/GCE has potential practical application for the detection of phosphite. Further, based on standard addition method, besides Fuzhou Minjiang River (China), the real sample from Fuzhou Xiyuan stream (China) was collected and prepared in the same way as Minjiang River. Whether it's Xiyuan stream or Minjiang River, no phosphite was detected.

## 3. Conclusion

In summary, UiO-66/GO composites were successfully prepared and first used to construct an electrochemical sensor for effectively detecting P (III) in the presence of P(V). The developed sensor exhibits a wide detection range of 10 μmol $L^{-1}$-500 μmol $L^{-1}$, with a lowest LOD of 0.33 μmol $L^{-1}$ (S/N = 3) among the reported phosphite electrochemical sensors. This work not only proposed a feasible strategy for effective detecting the phosphite in actual environment, but also provided a potential avenue for developing MOFs hybrid material use in electrochemical sensors for inorganic acid ion.

**Table 2.** Determination of phosphite in water samples.

| Added (μmol $L^{-1}$) | Found (μmol $L^{-1}$) | RSD (%) | Recovery |
|---|---|---|---|
| Minjiang River | ND | – | – |
| 10 | 9.87 ± 0.32 | 3.24 | 98.7 |
| 20 | 19.86 ± 0.51 | 2.56 | 99.3 |
| 50 | 48.96 ± 1.89 | 3.86 | 97.9 |
| Xiyuan Stream | ND | – | – |

SD: standard deviation; ND: not detected; RSD: relative standard deviation.

## Supporting Information Summary

Experimental details are presented in the Supporting Information. Supporting Information is available from the Wiley Online Library.

## Acknowledgements

*The authors gratefully acknowledge the financial supports of the National Natural Science Foundation of China (21971038, 21975044 and 21805039) and Natural Science Foundation of Fujian Province (2018 J07001 and 2019H6012).*

## Conflict of Interest

The authors declare no conflict of interest.

**Keywords:** Electrochemistry · Graphene oxide · Metal-organic frameworks · Phosphite · Sensor

[1] a) N. Chen, Y. Wu, Z. Chen, H. Hong, *Estuar. Coast. Shelf Sci.* **2015**, *166*, 178–188; b) A. Paytan, K. Mclaughlin, *Chem. Rev.* **2007**, *107*, 563–576.
[2] G. Keglevich, E. Bálint, *Molecules* **2012**, *17*, 12821–12835.
[3] a) A. E. Mcdonald, B. R. Grant, W. C. Plaxton, *J. Plant Nutr.* **2001**, *24*, 1505–1519; b) P. Scott, P. A. Barber, G. E. S. J. Hardy, *Australas. Plant Path.* **2015**, *44*, 431–436.
[4] X. Yu, J. Geng, H. Ren, H. Chao, H. Qiu, *Environ. Sci-Proc. Imp.* **2015**, *17*, 441–447.
[5] P. R. Dametto, V. P. Franzini, J. A. G. Neto, *J. Agric. Food Chem.* **2007**, *55*, 5980–5983.
[6] a) C. Han, J. Geng, X. Xie, X. Wang, H. Ren, S. Gao, *Environ. Sci. Technol.* **2012**, *46*, 10667–10674; b) G. H. P. Roos, C. Loane, B. Dell, G. Hardy, *Commun. Soil Sci. Plant Anal.* **1999**, *30*, 2323–2329.
[7] a) H. Pech, A. Henry, C. S. Khachikian, T. M. Salmassi, G. Hanrahan, K. L. Foster, *Environ. Sci. Technol.* **2009**, *43*, 7671–7675; b) K. Breuzovska, A. Dimitrovska, Z. Kitanovski, J. Petrusevska, J. Tonic Ribarska, S. Trajkovic-Jolevska, *J. AOAC Int.* **2010**, *93*, 1113–1120.
[8] a) Y. Chang, M. Liu, J. Liu, *Anal. Chem.* **2020**, *92*, 3118–3124; b) S. Josiane de Lima, M. Neiva, O. Silvana Ruella de, L. Cleber Antonio, *Acta Sci. Technol.* **2008**, *30*, 231–236; c) H. A. Ito, M. F. de Oliveira, J. A. G. Neto, N. R. Stradiotto, *Ecletica. Quim. J.* **2002**, *27*, 161–168.
[9] O. Berkowitz, R. Jost, S. J. Pearse, H. Lambers, P. M. Finnegan, G. E. S. J. Hardy, P. A. O'Brien, *Anal. Biochem.* **2011**, *412*, 74–78.
[10] a) L. Liu, Z. Yao, Y. Ye, Y. Yang, Q. Lin, Z. Zhang, M. O'Keeffe, S. Xiang, *J. Am. Chem. Soc.* **2020**, *142*, 9258–9266; b) M. Y. Masoomi, A. Morsali, A. Dhakshinamoorthy, H. Garcia, *Angew. Chem. Int. Ed.* **2019**, *58*, 15188–15205.
[11] a) M. Ghorbanloo, V. Safarifard, A. Morsali, *New J. Chem.* **2017**, *41*, 3957–3965; b) Y. Xu, Q. Li, H. Xue, H. Pang, *Coord. Chem. Rev.* **2018**, *376*, 292–318; c) D. Sun, P. R. Adiyala, S. Yim, D. Kim, *Angew. Chem.* **2019**, *58*, 7405–7409; d) C. Liu, J. Li, H. Pang, *Coord. Chem. Rev.* **2020**, *410*, 213222.
[12] a) S. Friebe, B. Geppert, F. Steinbach, J. Caro, *ACS Appl. Mater. Interfaces.* **2017**, *9*, 12878–12885; b) F. Yang, W. Li, B. Tang, *J. Alloys Compd.* **2018**, *733*, 8–14; c) M. Yuan, X. Guo, N. Li, Q. Li, S. Wang, C. Liu, H. Pang, *Sens. Actuators. B Chem.* **2019**, *297*, 126809; d) M. Zhang, M. Li, W. Wu, J. Chen, X. Ma, Z. Zhang, S. Xiang, *New J. Chem.* **2019**, *43*, 3913–3920.
[13] a) B. Bozbiyik, T. Duerinck, J. Lannoeye, D. E. De Vos, G. V. Baron, J. F. M. Denayer, *Microporous Mesoporous Mater.* **2014**, *183*, 143–149; b) X. Zhang, Y. Yang, W. Huang, Y. Yang, Y. Wang, C. He, N. Liu, M. Wu, L. Tang, *Mater. Res. Bull.* **2018**, *99*, 349–358.
[14] Y. Ye, L. Gong, S. Xiang, Z. Zhang, B. Chen, *Adv. Mater.* **2020**, *32*, 1907090.

[15] a) M. Deng, S. Lin, X. Bo, L. Guo, *Talanta* **2017**, *174*, 527–538; b) N. Karimian, H. Fakhri, S. Amidi, A. Hajian, F. Arduini, H. Bagheri, *New J. Chem.* **2019**, *43*, 2600–2609.
[16] H. Qiu, M. Ye, Q. Zeng, W. Li, J. D. Fortner, L. Liu, L. Yang, *Chem. Eng. J.* **2019**, *360*, 621–630.
[17] a) S. Kempahanumakkagari, K. Vellingiri, A. Deep, E. E. Kwon, N. Bolan, K. Kim, *Coord. Chem. Rev.* **2018**, *357*, 105–129; b) A. Amini, S. Kazemi, V. Safarifard, *Polyhedron* **2020**, *177*, 114260.
[18] a) X. Sun, Z. Liu, K. Welsher, J. T. Robinson, A. Goodwin, S. Zaric, H. Dai, *Nano Res.* **2008**, *1*, 203–212; b) L. Zhang, J. Xia, Q. Zhao, L. Liu, Z. Zhang, *Small* **2010**, *6*, 537–544.
[19] a) H. Guo, T. Jiao, Q. Zhang, W. Guo, Q. Peng, X. Yan, *Nanoscale Res. Lett.* **2015**, *10*, 272; b) G. Zhou, Z. Wang, W. Li, Q. Yao, D. Zhang, *Mater. Lett.* **2015**, *156*, 205–208.
[20] a) S. Feng, Y. Yang, M. Li, J. Wang, Z. Cheng, J. Li, G. Ji, G. Yin, F. Song, Z. Wang, *ACS Appl. Mater. Interfaces.* **2016**, *8*, 14503–14512; b) D. Lee, S. Na, S. Kim, *Nanoscale* **2016**, *8*, 1513–1522.
[21] W. Yi, Z. He, J. Fei, X. He, *RSC Adv.* **2019**, *9*, 17325–17334.
[22] Y. Shen, Z. Li, L. Wang, Y. Ye, Q. Liu, X. Ma, Q. Chen, Z. Zhang, S. Xiang, *J. Mater. Chem.* **2015**, *3*, 593–599.
[23] H. Sun, B. Tang, P. Wu, *ACS Appl. Mater. Interfaces.* **2017**, *9*, 26077–26087.
[24] X. Wang, Q. Wang, Q. Wang, F. Gao, F. Gao, Y. Yang, H. Guo, *ACS Appl. Mater. Interfaces.* **2014**, *6*, 11573–11580.
[25] B. Shan, S. M. Mcintyre, M. R. Armstrong, Y. Shen, B. Mu, *Ind. Eng. Chem. Res.* **2018**, *57*, 14233–14241.
[26] S. Trasatti, A. Alberti, *J. Electroanal. Chem.* **1966**, *12*, 236–249.
[27] Q. Guan, B. Wang, X. Chai, J. Liu, J. Gu, P. Ning, *Fuel* **2017**, *205*, 130–141.
[28] P. Zhao, N. Liu, C. Jin, H. Chen, Z. Zhang, L. Zhao, P. Cheng, Y. Chen, *Inorg. Chem.* **2019**, *58*, 8787–8792.
[29] a) P. Lu, Y. Wu, H. Kang, H. Wei, H. Liu, M. Fang, *J. Mater. Chem. A* **2014**, *2*, 16250–16267; b) S. Wang, J. Wang, W. Cheng, X. Yang, Z. Zhang, Y. Xu, H. Liu, Y. Wu, M. Fang, *Dalton Trans.* **2015**, *44*, 8049–8061.
[30] C. X. Fan, L. Zhang, L. Y. Yang, W. Y. Huang, P. Z. Xu, *Oceanologia et Limnologia Sinica.* **2002**, *33*, 370–378. (In Chinese)
[31] S. Zheng, D. Wu, L. Huang, M. Zhang, X. Ma, Z. Zhang, S. Xiang, *J. Appl. Electrochem.* **2019**, *49*, 563–574.

Submitted: June 29, 2020
Accepted: September 4, 2020